Block Length Dependence of Morphological Phase Diagrams of the Ternary System of PS-*b*-PAA/Dioxane/H_2O

Hongwei Shen and Adi Eisenberg*

Department of Chemistry, McGill University, 801 Sherbrooke Street West, Montreal, Quebec, Canada H3A 2K6

Received July 16, 1999

ABSTRACT: The block length dependence of the morphological phase diagram was investigated for PS-*b*-PAA copolymers in dioxane/water using transmission electron microscopy and light scattering techniques. The study was performed on copolymers with PS block lengths ranging from 49 to 310 repeat units and PAA block lengths from 7.2 to 26 repeat units. The water content ranged from 0 to 50 wt % and the copolymer concentration from 0 to 10 wt %. For all the copolymers with increasing water content, the sequence of morphologies, in general, follows the order of single chains, spheres, sphere and rod mixtures, rods, rod and bilayer mixtures, pure bilayers, and finally mixtures of bilayers and inverted structures. The bilayers here include vesicles, lamellae, and more complicated structures. It was found that the boundaries of various morphological transitions generally shift to lower water contents with increasing total block length and with decreasing PAA block length. Most importantly, it was found that long core-forming blocks and high water contents favor the formation of vesicles and that short core-forming blocks and low water contents favor open bilayers (e.g., lamellae). This finding suggests that in block copolymer systems the increase of bending modulus favors vesicle formation, which reinforces the conclusion of a theoretical study for mixed small molecule surfactant systems. The Gibbs free energies for the single chain to sphere transition were also estimated from the morphological phase diagram. It was found that at the same water content the free energy becomes less negative both with decreasing total block length and with increasing PAA block length.

1. Introduction

It has been known for many years that block copolymers can self-assemble to form micellar structures in selective solvents.[1] These micellar structures are generally spherical. Recent studies revealed that the aggregation of copolymers with a relatively long core-forming block can frequently lead to aggregates of various morphologies.[2−10] These morphologies include spheres, rods, lamellae, vesicles, large compound micelles (LCMs), large compound vesicles (LCVs), hexagonally packed hollow hoops (HHHs), and other complicated or inverted structures.[9] The effects of various factors, e.g., the composition of the block copolymers, the copolymer concentration, the type of the common solvent, the type and concentration of added ions, and temperature, have been explored to some extent.[8] Due to the increasing interest in the block copolymer aggregates of various morphologies, many aspects involving the formation of these aggregates, such as regions of stability of the various structures[10] and kinetics and mechanisms of the morphological transitions,[11] are currently under investigation.

The thermodynamics and kinetics of phase transitions of block copolymers in bulk[12] and of small molecule surfactants in solution[13] have been studied extensively. The phase behavior of such systems is relatively well understood. Both systems include two cubic, two hexagonally packed cylinder, two bicontinuous cubic, and one lamellar ordered phase. For the small molecule surfactant systems, in addition to the ordered structures, various morphologies, such as spheres, rods, irregular bicontinuous, and open bilayers or even vesicles, also appear in the disordered phase.[13,14] It should be noted that, in general, not all the phases mentioned above are present in any one system. One series of copolymers, i.e., those based on poly(ethylene oxide) (PEO), has been studied intensively in solution for some years.[15,16] The phase behavior is similar to that of copolymers in bulk. It was suggested that similar principles govern the phase behavior of block copolymers in bulk and in concentrated or semidilute solution and even of small molecule surfactant systems.[16]

In our first study on the morphological phase diagram of the diblock PS_{310}-*b*-PAA_{52} in dioxane/water, we utilized freeze-drying transmission electron microscopy (TEM), turbidity measurements, and static and dynamic light scattering.[10] Due to the relatively high freezing points of both water and dioxane, aggregate morphologies were preserved by quenching and subsequent freeze-drying of solution samples; the structures were then observed using TEM. It was found that spheres, rods, and vesicles are all equilibrium morphologies prior to quenching. It was also found that, with increasing water content, the sequence of copolymer structures in solution follows the order of single chains, spheres, sphere and rod mixtures, rods, rod and vesicle mixtures, and finally vesicles. Not only the water content but also the polymer concentration and homopolystyrene content influence the morphologies and the sizes of the aggregates. Also, the Gibbs free energies of the various morphological transitions were estimated from the positions of the morphological boundaries. The first phase diagram study showed that the freeze-drying TEM technique is very useful in exploring the morphological behavior of block copolymers in solution.

The equilibrium nature of the morphologies observed here is analogous to that in bulk copolymer systems. For example, for PS−PI diblocks, the materials are at

* To whom correspondence should be addressed. E-mail: eisenber@chemistry.mcgill.ca.

10.1021/ma991161u CCC: $19.00
Published on Web 03/16/2000

Table 1. Molecular Characteristics of Diblock Copolymers and Aggregation Properties of the Copolymers in Solution

copolymer[a]	M_w/M_n[b]	PAA cont (%)[c]	CWC (1.00 wt %)	b[d]	R_h (nm) (1 wt % polym)	R_{h0} (nm) (40 wt % H_2O)
PS_{310}-*b*-PAA_{52}	1.05	14	8.5	1.60	20	450
PS_{132}-*b*-PAA_{16}	1.07	11	10.0	2.74	30	630
PS_{132}-*b*-PAA_{20}	1.07	13	11.0	2.73	40	330
PS_{132}-*b*-PAA_{26}	1.07	17	11.9	2.58	55	310
PS_{49}-*b*-$PAA_{7.2}$	1.15	13	13.5	3.27	70	250
PS_{49}-*b*-PAA_{10}	1.15	17	15.2	3.28	90	200

[a] The subscript labels represent the repeat units of the styrene block and the acrylic acid block. [b] The value of M_w/M_n represents the polydispersity of the diblock, where M_w is the weight-average molecular weight and M_n is the number-average molecular weight. [c] PAA content is defined as the percentage of acrylic acid units over the total units of the monomers. [d] b is the slope of the micellization curve shown in Figure 2.

equilibrium at high temperature and are then rapidly quenched to room temperature. At the time of observation, e.g., under an electron microscope, the structures are certainly not at equilibrium. One can, nevertheless, speak of equilibrium morphologies because that was what they were before quenching, and the quenching process did not alter the morphologies because morphological relaxation times are too long. Our systems represent equilibrium morphologies in the exactly same sense in that they were at equilibrium before quenching. Since the quenching time is of the order of a second or less, while the morphological relaxation times are at least of the order of minutes, and very much longer than the quenching time, we are describing equilibrium morphologies. It is worth noting that under some conditions nonequilibrium morphologies can be achieved in solution also. For example, a large increase in the water content, e.g., from 20 to 30 wt %, slows down the morphological relaxation times drastically, so waiting even for a few hours may not be enough to reach equilibrium. Such conditions were avoided in the present study of the equilibrium morphologies.

Thus, to ensure that morphologies are, indeed, at equilibrium, we performed a range of experiments. First, we studied the reversibility of the transitions from spheres to rods and then to vesicles and found them to be reversible with regard to not only the morphologies themselves but also the average diameters of spheres, rods, and vesicles. Furthermore, we stored the samples under conditions where morphological relaxation times are of order of minutes for a period up to 3 years and found no change of the morphologies. Finally, we heated samples of several morphologies to temperatures as high as 90 °C, kept them at that temperature for several hours, and on cooling obtained morphologies identical as those before the heating started. All of these experiments suggest that morphologies we referred to as "equilibrium morphologies" do, indeed, represent equilibria. Those morphologies that result in from insufficient waiting time, following experiments such as large water content jumps, will be referred to as nonequilibrium morphologies. The experiments described above were reported before.[10]

The above study also showed that vesicles can be formed spontaneously in high molecular weight block copolymer systems, as suggested in a theoretical study (SPA model).[17] That study dealt with a mixture of two surfactants, which individually form either micelles or lamellae. It was found that complexing interactions of the surfactants lead to nonideal mixing of surfactants on two sides of bilayers, and thus the effective bending modulus is negative in this type of system. Therefore, in a system with a bending modulus much larger than the temperature ($K \gg T$), vesicles are more stable than planar lamellae.

In our system, it is the polydispersity (heterogeneity) of the corona block of the block copolymers that is responsible for vesicle formation, a role that is played by complexing interactions in the mixed surfactant systems. Thus, polymer chains of different lengths can be unevenly distributed at two sides of the bilayers,[10] without the involvement of complexing interactions. The effective bending modulus should also be negative in our system and thus have the same effect on bilayer structures as that in mixed surfactant systems. Since the bending moduli of polymers increase with increasing molecular weight, vesicles should be easier to form in long chain copolymer systems and more difficult to form in short chain copolymer systems.

One of the aims of the present study is to test whether the increase of the bending modulus of polymer favors vesicle formation. More generally, in the present paper, we describe the block length dependence of the morphological phase diagram of the ternary system PS-*b*-PAA/dioxane/water. The study was performed using freeze-drying TEM and light scattering techniques for copolymers with PS blocks ranging from 49 to 310 repeat units and PAA blocks in the range of 7.2−26 units. The water content ranged from 0 to 50 wt % and polymer concentration from 0.1 to 10 wt %. The total block length effect was studied using copolymers with a similar composition, while the PAA effect was investigated using copolymers with the same PS block length. It was found that the morphological boundaries, in general, move to higher water contents with decreasing total block length and with increasing PAA block length. It was also found that long chain copolymers and high water contents favor the formation of vesicles and that planar lamellae are favored for short chain copolymers at relatively low water contents. An estimate of the Gibbs free energies for the single-chain/sphere transition is also given in the paper.

2. Experimental Section

2.1. Block Copolymers. The polystyrene-*b*-poly(*tert*-butyl acrylate) diblock copolymers were synthesized by sequential anionic polymerization of styrene followed by *tert*-butyl acrylate (*t*-BuA) using *sec*-butyllithium as the initiator,[18] following the method developed by Teyssié's group.[19] The poly(*t*-BuA) blocks in the copolymers were hydrolyzed to their acid form in toluene using *p*-toluenesulfonic acid as the catalyst. The homopolymers and diblocks were characterized using gel permeation chromatography (GPC) and FT-IR. A fractionation process was used to remove homopolystyrene from the diblocks. A detailed description of the procedures can be found elsewhere.[18] The copolymers used in the present study are listed in Table 1.

2.2. Light Scattering. The light scattering experiments were performed on a Brookhaven light scattering instrument with a BI9000 AT digital correlator. The instrument is equipped with an Uniphase μBlue laser, which supplies

vertically polarized light with a wavelength of 532 nm. The experiments were performed by monitoring the scattered light intensity at a 90° scattering angle at 25 °C. Stock solutions (1−10 wt % of copolymer) were prepared by dissolving the diblocks in dioxane and were then stored overnight in covered glass tubes sealed with Teflon tape. These stock solutions were filtered directly into scintillation vials of a diameter of 1.5 cm and diluted with filtered dioxane solvent to the desired copolymer concentrations. Then, filtered deionized water was added dropwise at a rate of 0.2 wt % per minute to form the aggregates. Static light scattering (SLS) measurements were performed after each sample had been allowed to equilibrate at a given water content for 20 min. Each of the water increments was ca. 1 wt %. Dynamic light scattering (DLS) measurements were also used in the present study. The data were taken at the same water content intervals as those in the phase diagram study (ca. 2 wt %).

2.3. Transmission Electron Microscopy. Transmission electron microscopy (TEM) was performed on a Phillips EM400 microscope operating at an acceleration voltage of 80 kV. For the observation of the aggregate morphologies, the sample was prepared in a similar way to that for SLS measurements (see section 2.2). Additionally, at each water interval (ca. 2 wt %), samples were stored for 3−7 days depending on the water content to ensure that true equilibria are reached. A drop of each sample was withdrawn from the solution and deposited onto a carbon-coated EM copper grid, which had been prepared previously.[10] The sample grid was then immediately frozen at a temperature near that of liquid nitrogen and freeze-dried as described previously.[10] Finally, the grid was shadowed at an angle of ca. 35° using Pd/Pt alloy before TEM observations.

3. Results and Discussion

The Results and Discussion section is divided into five parts. The first presents the morphological phase diagrams of six PS-*b*-PAA diblock copolymer systems. In the second and third parts, the effect of the total block length and the effect of the PAA block length on the morphological phase diagram are described, respectively. In both parts, the effects on both micellization curves and aggregate morphologies are discussed. A brief discussion on the PS block length effect is presented in the fourth part. Finally, the estimation of Gibbs free energies of the single chain to sphere transition is addressed.

3.1. Morphological Phase Diagrams. The morphological phase diagram for each copolymer system was obtained from ca. 100 samples using a previously established method.[10] The boundaries of various morphological transitions were estimated by drawing smooth lines between experimental points which represent different morphologies. For the sake of simplicity, the phase diagrams are presented in the present paper without showing the experimental points. An example of a phase diagram with experimental points can be found in the previous study.[10] Parts A, B, C, D, E, and F of Figure 1 show the morphological phase diagrams of fractionated copolymers PS_{310}-*b*-PAA_{52}, PS_{132}-*b*-PAA_{16}, PS_{132}-*b*-PAA_{20}, PS_{132}-*b*-PAA_{26}, PS_{49}-*b*-$PAA_{7.2}$, and PS_{49}-*b*-PAA_{10}, respectively. The solid lines are the boundaries determined from TEM pictures. The dotted line in Figure 1A is the micellization curve determined from SLS measurements (see section 3.2.1). Such lines were determined for all the phase diagrams, and their positions relative to the solid lines are similar. The letters S, R, B, V, and I represent spheres, rods, open bilayers, vesicles, and inverted structures, respectively. Combinations of letters stand for the corresponding mixed morphologies. The vesicle represents only one type of bilayer. Since different types of bilayers are encountered in this study, we differentiate vesicles from nonvesicular structures, which are referred to as open bilayers. For copolymer systems in which both vesicles and open bilayers are observed, a boundary is drawn between regions containing vesicles and those containing open bilayers. As seen from Figure 1, with increasing water content, the aggregate morphology in all the phase diagrams generally follows the order of spheres, sphere and rod mixtures, rods, rod and open bilayer or rod and vesicle mixtures, open bilayers or vesicles, and finally, for some copolymers, mixtures of open bilayers, vesicles, and inverted structures.

3.2. Effect of the Total Block Length. One of the aims of this study is to explore the difference in the phase diagrams for high molecular weight and low molecular weight copolymers. For any PS block length, the window of PAA block lengths needed to obtain morphologies other than small spherical micelles and large LCMs is limited. Therefore, the effect of the total block length on the morphological phase diagram was examined by keeping a similar ratio of the PAA block to the PS block. Two series of copolymers with different PAA contents were studied. One series consists of PS_{310}-*b*-PAA_{52}, PS_{132}-*b*-PAA_{20}, and PS_{49}-*b*-$PAA_{7.2}$, which have a PAA content of ca. 13% (see Table 1). Their phase diagrams are shown in parts A, C, and E of Figure 1. The simplified phase diagram of the copolymer PS_{310}-*b*-PAA_{52} (Figure 1A) is also presented here to facilitate the comparison of the various phase diagrams, although a complete diagram for that system, with experimental points, has been shown before.[10] The other series, with a PAA content of 17%, includes PS_{132}-*b*-PAA_{26} and PS_{49}-*b*-PAA_{10}; their phase diagrams are presented in parts D and F of Figure 1, respectively. One could also consider the series of copolymers containing PS_{132} block as well as the series containing PS_{49} block as additional series. The last two series will be discussed in section 3.3.

3.2.1. Single-Chain/Sphere Boundary and Micellization Curve. As seen from Figure 1, the single-chain/sphere boundary at the onset of aggregation moves to higher water contents with decreasing total block length for both series of copolymers. For example, for the copolymer PS_{310}-*b*-PAA_{52} at 1.0 wt % of polymer, the single-chain/sphere boundary occurs at 6.9 wt % of water, while for PS_{132}-*b*-PAA_{20} and PS_{49}-*b*-$PAA_{7.2}$ at the same polymer concentration, the boundary appears at 9.0 and 11.0 wt % of water, respectively. As the PS block length decreases, the interfacial tension decreases, and the morphological boundaries move to higher water contents.[5] Because the effect is examined by keeping a constant PAA content in the copolymers, the corona-forming block length also decreases in proportion to decreasing PS block; the decrease in the PAA block length, by itself, would cause the boundaries to move toward lower water contents. Since the boundaries, in fact, move to higher water contents, the effect of shortening the PS block obviously dominates the behavior. In addition, all the boundaries shift to higher water contents with decreasing polymer concentration, as was also seen in the previous study.[10]

The micellization curves (e.g., dotted line in Figure 1A) determined from SLS measurements show similar trends as the single-chain/sphere boundaries, but they are not parallel to the single-chain/sphere boundaries. Additionally, all the micellization curves lie at higher water contents than the single-chain/sphere boundaries,

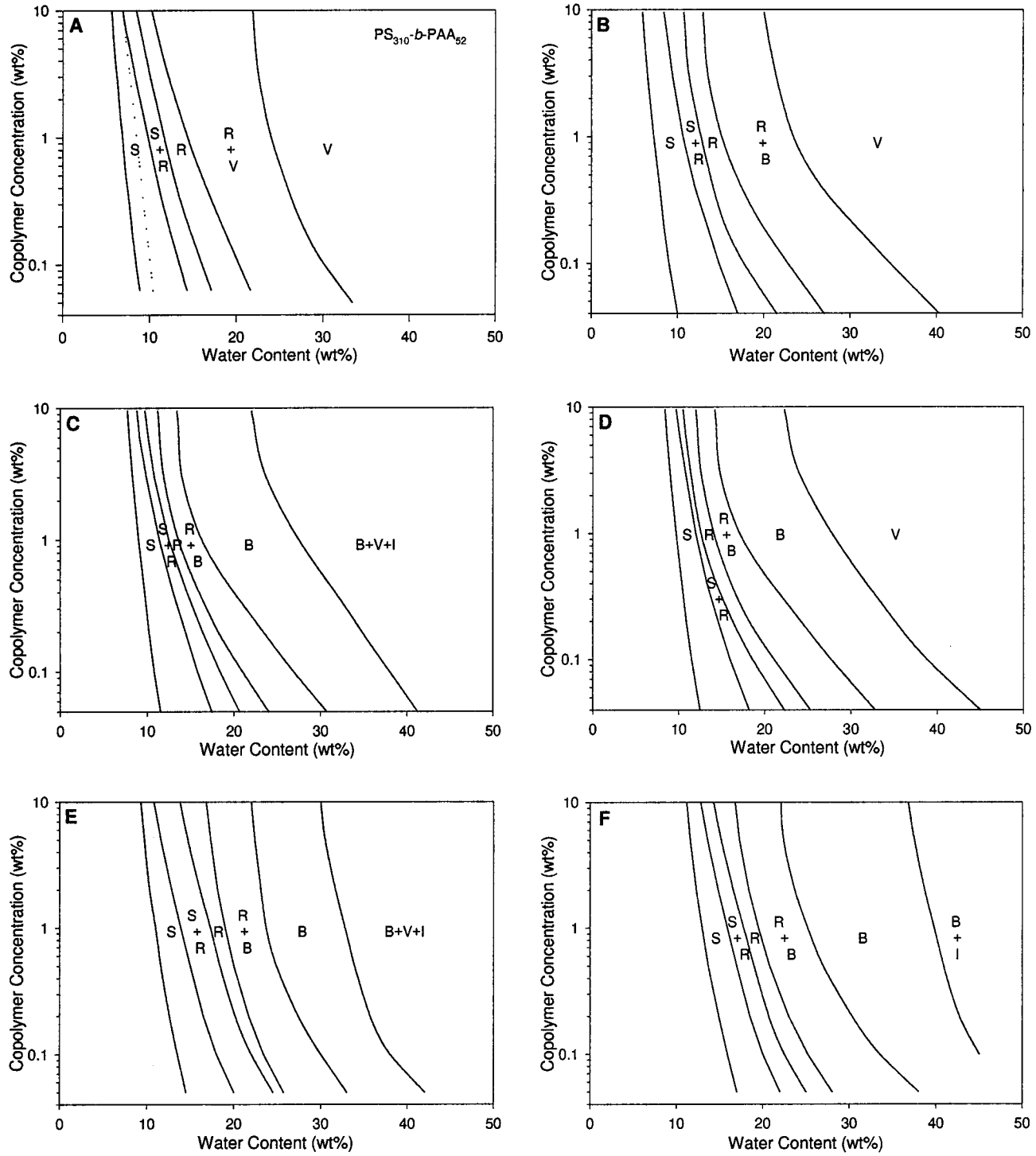

Figure 1. Morphological phase diagrams for the ternary system of the diblock PS-*b*-PAA/dioxane/water. Solid lines are the boundaries that are drawn between experimental points. The dotted line represents the micellization curve determined form SLS measurements. The letters S, R, B, V, and I represent spheres, rods, open bilayers, vesicles, and inverted structures, respectively. Combinations of letters stand for corresponding mixed morphologies.

which is, again, consistent with the previous study.[10] To demonstrate the effect of the total block length on the micellization curve, Figure 2 presents the micellization curves for all the copolymers on a plot of the critical water content (CWC) against the logarithm of the polymer concentration. All the plots are linear with $r^2 > 0.99$. Circles and squares represent the results for copolymers with ca. 13% and 17% PAA, respectively. It is clear that the micellization curves move to higher water contents as the total block length decreases. The slopes of the micellization curves, listed in Table 1, increase slightly with decreasing total block length. Using the previously established method,[10] the fraction of aggregated polymer chains $[(C - \mathrm{cmc})/C]$ in the total polymer can be estimated from

$$(C - \mathrm{cmc})/C = 1 - \exp[-2.303([H_2O] - \mathrm{CWC})/b] \quad (1)$$

where C and cmc are the total polymer concentration after dilution and the critical micellization concentration, respectively; $[H_2O]$ represents the water content, and b is the slope of the micellization curve listed in

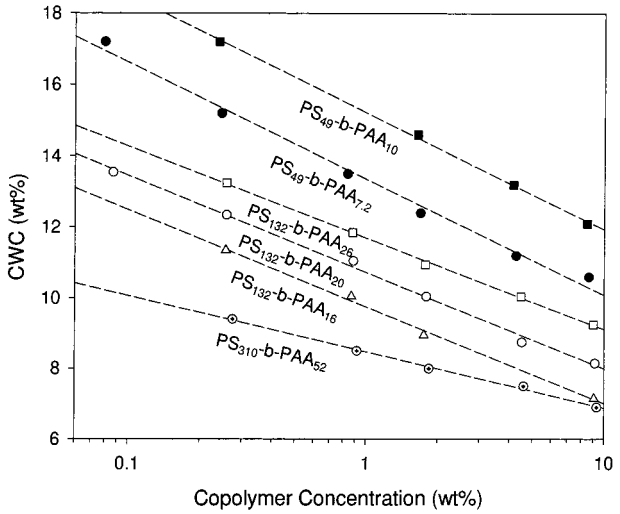

Figure 2. Micellization curves determined from SLS measurements by plotting the CWC against the logarithm of the polymer concentration.

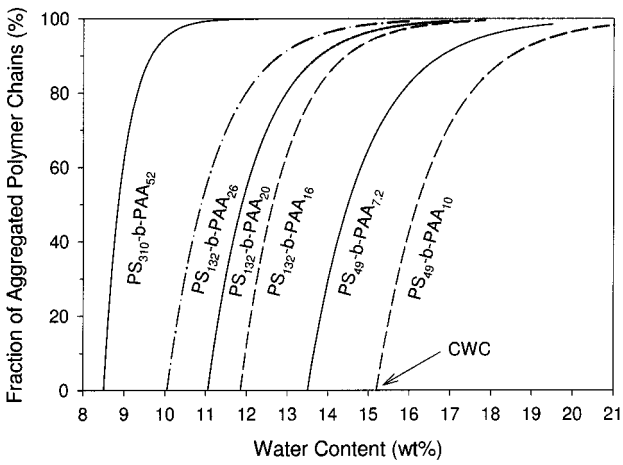

Figure 3. Fraction of aggregated polymer chains as a function of the water content for 1.00 wt % polymer. All the curves start at their CWCs on the *x*-axis.

Table 1. The fraction of the single chains in the total copolymer can then be obtained by subtracting the fraction of the aggregated polymer chains from 1.

Figure 3 shows the fraction of aggregated polymer chains as a function of the water content for 1.00 wt % of block copolymers. The CWC of each sample is also listed in Table 1. The solid lines and dashed lines represent copolymers with ca. 13% and 17% PAA, respectively. The dash−dotted line represents the copolymer PS_{132}-*b*-PAA_{16}, which will be discussed in section 3.3.1. Figure 3 also illustrates the block length dependence of the single chain fraction as a function of the water content. As seen in the figure, for the long chain copolymer PS_{310}-*b*-PAA_{52}, the fraction of aggregated polymer chains increases sharply after the onset of aggregation at 8.5 wt % water (its CWC) to ca. 99% at ca. 11 wt % water; by contrast, it increases more slowly for the short chain copolymer PS_{49}-*b*-$PAA_{7.2}$ from its cmc (13.5 wt % water) to 99% aggregation at ca. 21 wt % water. In the previous study, we have shown that various aggregates prepared from the long chain copolymer PS_{310}-*b*-PAA_{52} are equilibrium structures.[10] For copolymers with shorter chains, single chain fractions are higher and the chain exchange dynamics are faster.[20] Therefore, it is very likely that the aggregates prepared under the same conditions from these copolymers are also equilibrium structures.

3.2.2. Boundaries of Other Morphological Transitions. For the copolymer series containing samples with ca. 13% PAA (see Figure 1A,C,E) and that containing polymers with 17% PAA (see Figure 1D,F), as the PS block length decreases, the sphere/sphere + rod and sphere + rod/rod boundaries move to relatively higher water contents, in parallel with the movement of the single-chain/sphere boundary. The boundaries involving bilayer structures show more complicated behavior. In general, all the corresponding boundaries move to higher water contents with decreasing total block length. This can be seen from Figures 1D,F and 1C,E. For the copolymer PS_{310}-*b*-PAA_{52} (Figure 1A), however, the behavior is different because, right after the rods, vesicles appear rather than open bilayers. In comparing the rod/rod + vesicle boundary in Figure 1A with the rod/rod + open-bilayer boundary in Figure 1C,E, it is found that the boundary in Figure 1A appears at higher water contents than the one for the copolymer PS_{132}-*b*-PAA_{20} (Figure 1C). Also, the rod + vesicle/vesicle boundary in Figure 1A stays at higher water contents than the rod + open-bilayer/open-bilayer boundary in Figure 1C.

The general behavior of the corresponding boundaries involving bilayer structures shows the same type of behavior as the single-chain/sphere boundary (see section 3.2.1), i.e., the movement to higher water contents with decreasing total block length at a constant composition. It is quite possible, however, that quantitatively the effect of decreasing the PS block length might not be exactly equal to that of increasing PAA block length. Thus, over wider block length ranges, one or the other of these factors predominates even at a constant composition. The relative positions of the boundaries might be due to such a difference.

3.2.3. Various Morphologies Involving Bilayer Structures. The SPA model suggested that in mixed surfactant systems the higher the bending modulus, the easier the formation of vesicles.[17] Because of the uneven distribution of different copolymer chains at two sides of bilayers, the change of the bending modulus may also have the same effect on vesicle formation for block copolymer systems. Thus, vesicles should form more easily from high molecular weight block copolymers, since the bending modulus increases with increasing molecular weight of copolymers. Our previous study of the copolymer PS_{310}-*b*-PAA_{52} has demonstrated the spontaneous formation of vesicles.[10] A study of the morphologies of copolymers with shorter total block lengths but a similar PAA content can check the effect of bending modulus on bilayer structures for our system. In addition, such a study may provide an extension of the range of control of the morphologies and sizes of aggregates.

As seen from Figure 1, at relatively high water contents, the bilayer structures seen for copolymers with relatively short blocks (e.g., PS_{49}-*b*-$PAA_{7.2}$) are open bilayers, which are significantly different from the vesicles (or closed bilayers) observed for long chain copolymers (e.g., PS_{310}-*b*-PAA_{52}). However, the change in the total block length does not affect the relative position or sequence of the various morphologies in the phase diagram at relatively low water contents. Spheres and rods always appear first. The next two graphs will show graphically not only the block length effect but

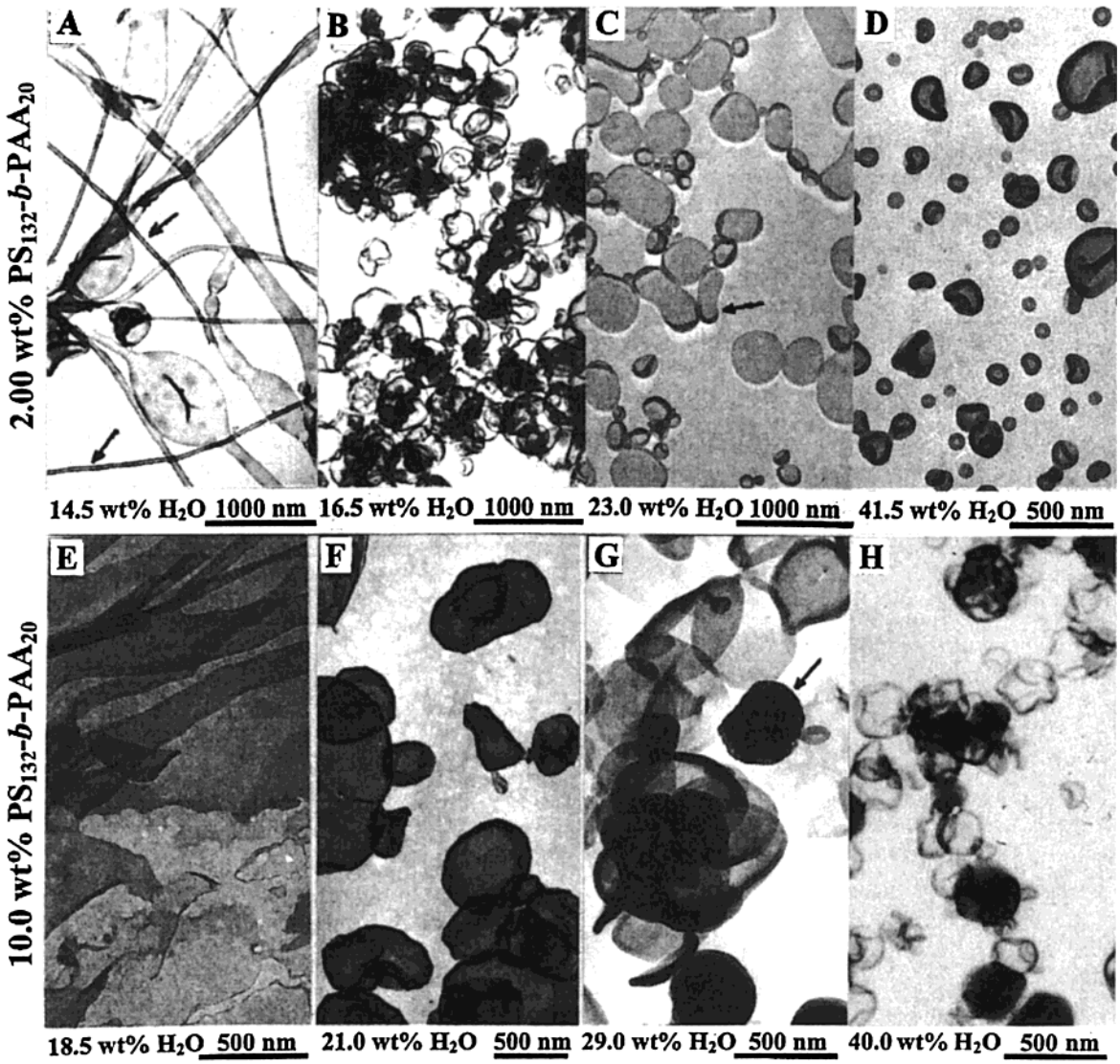

Figure 4. Aggregate morphology as a function of the water content for 2.00 and 10.0 wt % of the copolymer PS_{132}-*b*-PAA_{20}. The arrows indicate tubular structures in (A), lamellae with curved edges in (C), and HHH structures in (G).

also the water content and polymer concentration effects on bilayer structures, which are also significant.

Figure 4 shows the aggregate morphologies observed for the copolymer with the intermediate block length, i.e., PS_{132}-*b*-PAA_{20}, at various water contents for two polymer concentrations (2.00 and 10.0 wt %). The upper four pictures refer to a polymer concentration of 2.00 wt %; Figure 4A shows mixed open bilayers at a water content of 14.5 wt %, which is near the rod + open-bilayer/open-bilayer boundary in the phase diagram (see Figure 1C). Some of the bilayers are tubules (see arrows in the picture). Ribbons and a few irregular open bilayers are also seen. As the water content increases to 16.5 wt % water (in the open bilayer region), the various mixed bilayers change to somewhat more regular bilayers, shown in Figure 4B. The bilayer structures mostly change to disklike lamellae at 23.0 wt % water (see Figure 4C), which is close to the open-bilayer/open-bilayer + vesicle boundary. As seen from the shadows of the aggregates, some of the lamellae have curved edges, such as those indicated by arrows. With a further increase in the water content to 41.5 wt %, most of bilayers change to regular vesicles with a broad distribution of sizes, as shown in Figure 4D.

For a higher polymer concentration in the same copolymer, i.e., 10.0 wt %, more complicated morphologies appear (shown in the four lower pictures in Figure 4). Figure 4E shows large planar lamellae or wide ribbons appearing at a water content of 18.5 wt %, which is in the open bilayer region of the phase diagram (see Figure 1C). Some of the planar lamellae contain holes or other imperfection. In this region, the viscosity of the solution is also very high due to the presence of the large aggregates. This morphology, to some degree, is parallel to the ordered lamellar phase appearing in small molecular surfactant systems[13] or PEO-based copolymer systems.[15,16] These changes in morphologies are currently under investigation in detail. With increasing water content (to 21.0 wt %), the planar lamellae change to individual bilayer structures, some of which are collapsed to give irregular shapes, as shown in Figure 4F. These bilayer structures further change to a mixture of various structures at 29.0 wt % water, located in the mixture region of the phase diagram. Figure 4G shows this mixture of morphologies, which includes disklike lamellae, irregular shaped bilayers, and regularly packed inverted structures; the arrow indicates an example of such an inverted structure.

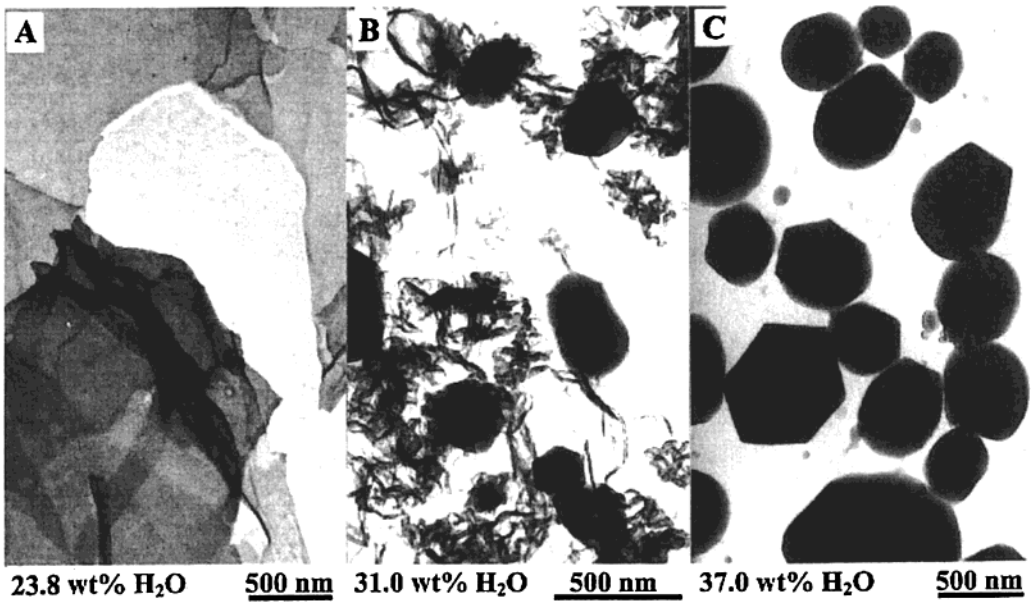

Figure 5. Morphologies as a function of the water content for 10.0 wt % of PS_{49}-*b*-$PAA_{7.2}$.

Judging from the packing pattern at the edge of the aggregates, and the outside shape of the aggregate, the inverted structures are probably of the HHH morphology.[6] At a still higher water content (41.0 wt %, Figure 4H), again a mixture of various morphologies, including vesicles, open bilayers, and HHHs, is seen. The difference in the aggregate morphologies between low and high polymer concentrations can be ascribed to the effect of the volume fraction of copolymers in solution, which is similar to that seen in small molecule surfactant systems.[13]

The effect of the water content on bilayer structures will now be discussed in the term of the effective bending modulus. For both copolymer concentrations shown in Figure 4, the bilayer structures tend to be generally planar at relatively low water contents. Because at low water contents dioxane is present in the core of the aggregate,[7] the glass transition temperature (T_g) of the core should be relatively low. As a result, the stiffness of the PS segments in the core should be low, along with the bending modulus. Thus, the bilayer structures should be planar, as seen in Figure 4A,E. With increasing water content, the dioxane concentration in the aggregate core decreases.[7] As a result, the stiffness of the PS chains in the core increases, along with the bending modulus of the core materials. Thus, the large planar bilayer structures break down into relatively smaller structures (see Figure 4B,F). A further increase in the water content results in even higher bending moduli and results in the appearance of vesicles (see Figure 4D,H).

For the copolymer PS_{49}-*b*-$PAA_{7.2}$, which has an even shorter total block length, the aggregate morphologies at 10.0 wt % polymer are again different, as shown in Figure 5. Figure 5A shows large planar lamellae formed at a water content of 23.8 wt % in the open bilayer region of the phase diagram (see Figure 1E). Although planar lamellae are also present for the copolymer PS_{132}-*b*-PAA_{20}, the lamellae are even larger in the present case. Figure 5B shows a mixture of irregular bilayer structures and some inverted structures at 31.0 wt % water, which is close to the boundary from open bilayers to a mixture of various morphologies (see Figure 1E). At a water content of 37.0 wt %, most of polymer is present in the form of the inverted structures, as shown in Figure 5C. The inverted morphologies are so compact that no internal structure can be seen, probably because of the very small diameters of the hollow rod regions that the short PAA blocks produce in the PS domain. A comparison of the outside shapes of the present aggregates to those of the inverted structures shown in Figure 4G and to those of the HHH morphology identified before[6] suggests that the present inverted structures are probably of the HHH morphology.

As discussed earlier, the water content affects the bending modulus and thus the appearance of the bilayer structures. Here, we focus on the effect of the total block length on the appearance of the bilayer structures at the beginning of the bilayer formation (relatively low water contents). Since the bending modulus is expected to decrease with decreasing molecular weight of block copolymers, the tendency to form vesicles will decrease with decreasing total block length. Therefore, the structure seen for the copolymer PS_{310}-*b*-PAA_{52} is the vesicle because the copolymer has a long total block length. For the copolymer PS_{132}-*b*-PAA_{20}, which has a shorter total block length, the bilayer structures change to irregular planar lamellae (see Figure 4A,F) due to the relatively lower bending modulus. For the copolymer PS_{49}-*b*-$PAA_{7.2}$, which has the shortest total block length, large planar lamellae appear (see Figure 5A) because of the lowest bending modulus. Therefore, to form stable vesicles, the total block length has to be long enough to provide a high bending modulus to stabilize the vesicular structure. It should be kept in mind that the increase in the total block length here is limited for copolymers with a narrow range of the PAA/PS ratios. This study provides the first experimental evidence to support that vesicles are favored for long chain block copolymer systems, while open bilayers are favored for short chain block copolymers.

Since at high water contents, pure vesicles appear at low polymer concentrations, the *z* average hydrodynamic radius (R_h) of the vesicles can be estimated from DLS measurements using the CONTIN method.[10] Figure 6 gives the plots of the inverse effective hydrodynamic radii against the polymer concentration at ca. 40 wt % water. Circles represent the results for copolymers

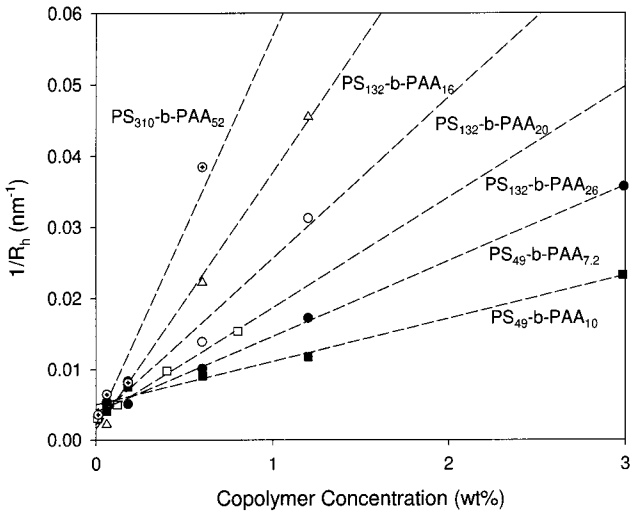

Figure 6. Plot of the inverse effective hydrodynamic radius against the polymer concentration.

with ca. 13% PAA content. As seen in Figure 6, the higher the total block length, the smaller the vesicle radius. Also, the effective hydrodynamic radii are strongly dependent on the polymer concentration; their values at 1 wt % polymer are listed in Table 1. It is clear that vesicles formed from short chain copolymers have large hydrodynamic radii and thus show the greatest tendency to form flat lamellae. This result again supports the theoretical study.[17] All the plots in Figure 6 can be fitted to straight lines with $r^2 > 0.98$. By extrapolating polymer concentration to zero, the *z* average hydrodynamic radii (R_{h0}) can then be obtained; they are listed in Table 1. The trends of R_{h0} with varying block lengths are different from those of the effective hydrodynamic radii, in that they show an inversion of the trends. It is interesting to note that for the PS_{132} series the inversion occurs at ca. 0.1 wt % polymer, at which the hydrodynamic radius is ca. 180 nm; for the PS_{49} series, the inversion takes place at ca. 0.2 wt % polymer with a corresponding hydrodynamic radius of ca. 170 nm. At these points, the radii are independent of the PAA block length.

To see whether the above morphological changes are general trends, it is essential to study the morphologies of the other series of copolymers, i.e., those with 17% PAA. Figure 7 shows bilayer structures of the copolymer PS_{132}-*b*-PAA_{26} at two polymer concentrations. At a low

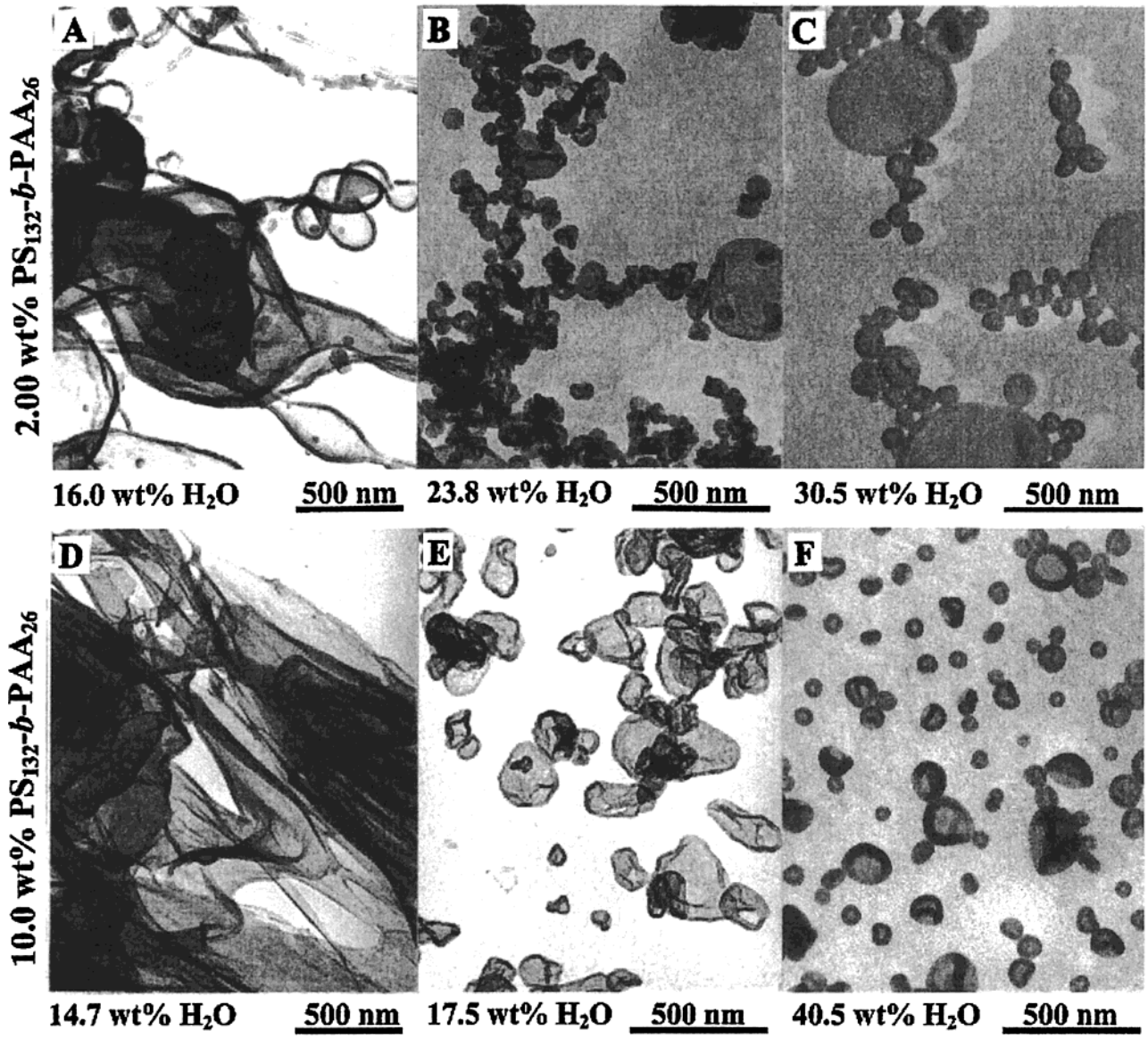

Figure 7. Morphologies at various water contents for 2.00 and 10.0 wt % of PS_{132}-*b*-PAA_{26}.

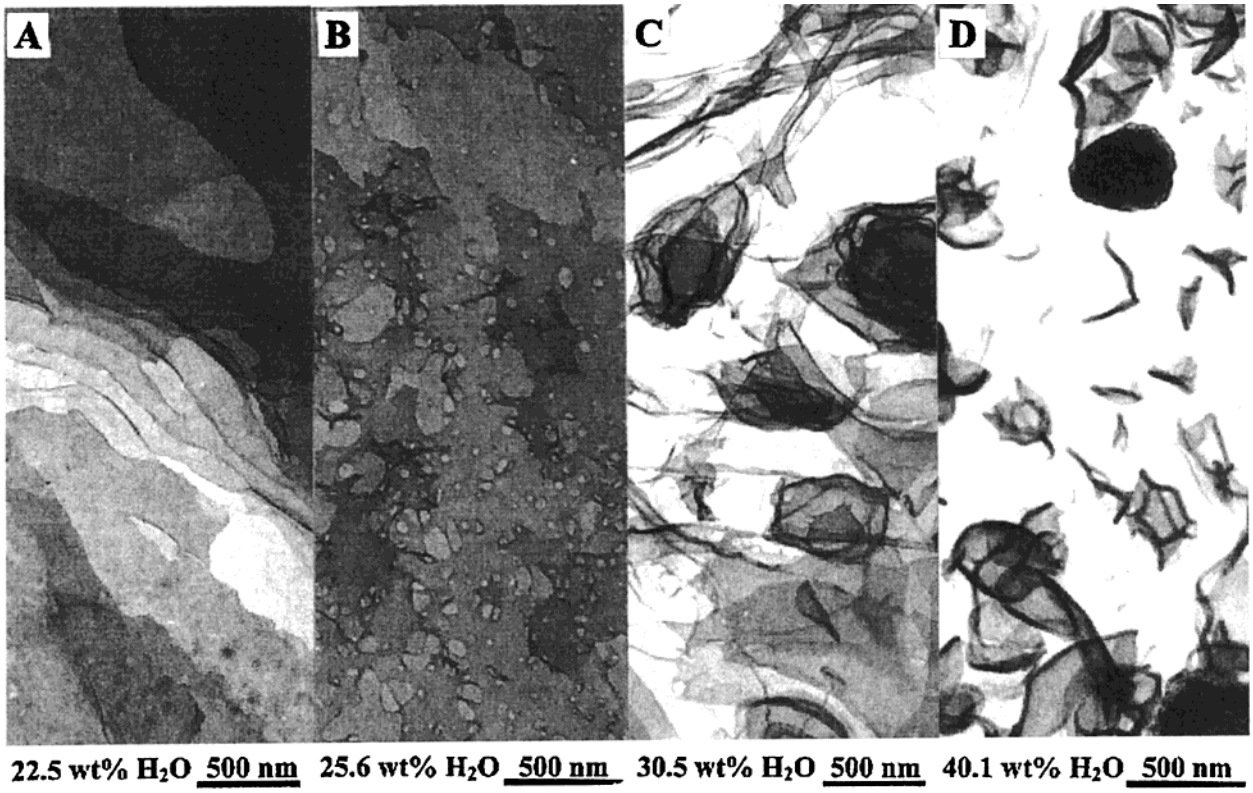

Figure 8. Morphologies for 10.0 wt % of PS_{49}-*b*-PAA_{10} in dioxane at various water contents.

polymer concentration (2.00 wt %, upper three pictures), irregular bilayers appear at 16.0 wt % water, as shown in Figure 7A. With increasing water content (to 23.8 wt %), the irregular bilayers change to smaller circular lamellae, some of which close up to form vesicles, as shown in Figure 7B. A further increase of the water content to 30.5 wt % causes more lamellae to form vesicles; the vesicular nature can be seen from the shadows of the aggregates in Figure 7C. When the polymer concentration increases to 10.0 wt % (lower three pictures in Figure 7), large bilayers are present at a water content of 14.7 wt %, as shown in Figure 7D. In some regions, the large bilayers are torn and twisted, presumably as a result of sample handling. With increasing water content (to 17.5 wt %), the large bilayers change to relatively smaller ones, as shown in Figure 7E. As the water content increases further to 40.5 wt %, most of the bilayers become vesicles, as seen in Figure 7F. The effects of changing the polymer concentration and changing the water content on the bilayer structures here show similar trends to those seen in the first series and can thus be considered general for that range of conditions.

The bilayer structures obtained at a polymer concentration of 10.0 wt %, for the shortest polymer studied here with 17% PAA, i.e., PS_{49}-*b*-PAA_{10}, are shown in Figure 8. At a water content of 22.5 wt %, flat layered lamellae are seen in Figure 8A. Also, at this stage, the viscosity of the solution is very high, and the solution shows a pinkish color, suggesting layering of the lamellae, which results in the formation of a gel with interlamellar spacing of the order of the wavelength of light. This structure is probably similar to the ordered lamellar phase in bulk copolymers,[12] in small molecule surfactant solutions,[13] and in PEO based copolymer solutions.[15,16] As the water content increases to 25.6 wt % (Figure 8B), some holes appear in the large planar lamellae. At a still higher water content (30.5 wt %), the lamellae change to irregular shapes and the overall aggregate sizes become smaller. The morphology is shown in Figure 8C. At this water content, the viscosity of the solution has decreased, suggesting that the gellike structure is in the process of breaking down. At a water content of 40.1 wt %, the gellike structure is no longer present and the viscosity of the solution is low. The aggregate morphology now consists of irregular bilayers with a few inverted structures, shown in Figure 8D. Obviously, the overall effect of the total block length on the bilayer structures for this series of copolymers (17% PAA) is the same as for the first series (ca. 13% PAA).

3.3. Effect of the PAA Block Length. The effect of the PAA block length on the morphological phase diagrams was investigated using two series of copolymers. One series has a PS block length of 132 repeat units of styrene and includes the copolymers PS_{132}-*b*-PAA_{16}, PS_{132}-*b*-PAA_{20}, and PS_{132}-*b*-PAA_{26}. The phase diagrams are shown in parts B, C, and D of Figure 1, respectively. The other series has two copolymers, PS_{49}-*b*-$PAA_{7.2}$ and PS_{49}-*b*-PAA_{10}. Figure 1E,F presents the phase diagrams of this second series. Because the PAA block length can affect the aggregate morphologies significantly, and because the various morphologies appear only for a narrow range of the PAA block lengths,[2] the present study only covers a narrow range of the PAA block length for the two PS block lengths.

3.3.1. Single-Chain/Sphere Boundary and Micellization Curve. For the series of copolymers with PS_{132}, as the PAA block length increases from 16 to 26, the single-chain/sphere boundary moves to higher water contents, as seen from Figure 1B,C,D. This is simply due to the increase of the solubility of the copolymer caused by the increased PAA block length. As seen from the open symbols in Figure 2, the micellization curve also shifts to higher water contents with increasing PAA

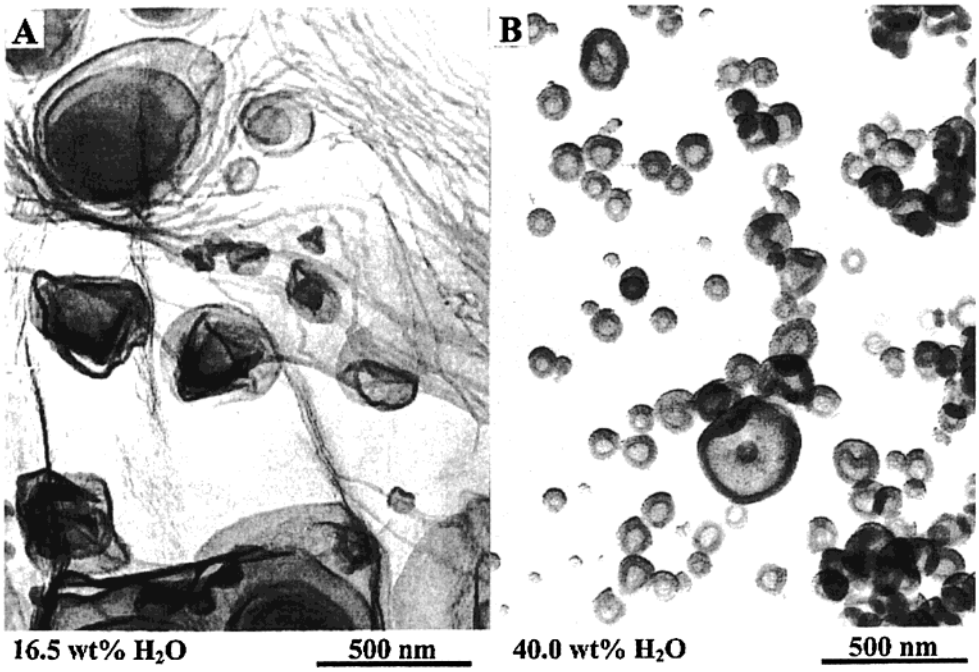

Figure 9. Morphologies of 10.0 wt % of PS_{132}-*b*-PAA_{16} in dioxane at two water contents.

block length, parallel to the effect of decreasing the total block length. The slopes of the micellization curves are nearly independent of the PAA block length within experimental error; they are primarily a function of the PS block length (see section 3.2.1). The fraction of aggregated polymer chains as a function of the water content shows a similar trend for different PAA block lengths, and only the *x*-axis intercept, or CWC, is different (see Figure 3). For example, for PS_{132}-*b*-PAA_{26}, the fraction of aggregated polymer chains increases from zero at 10.0 wt % water (the CWC) to 99% with in a 5 wt % water increment; for PS_{132}-*b*-PAA_{16}, it also takes a ca. 5 wt % water increment to increase the fraction to 99% from the CWC (at 11.9 wt % water).

For the series of copolymers with PS_{49}, the single-chain/sphere boundary also moves to higher water contents with increasing PAA block length, as seen in Figure 1E,F. As in the PS_{132} series, the two micellization curves are parallel to each other (see closed symbols in Figure 2). Again, the fraction of aggregated polymer chains as a function of the water content shows a similar profile, and only the *x*-axis intercept, or CWC, occurs at different water contents (see the two curves at the far right in Figure 3). Obviously, the effect of the PAA block length seen here parallels that seen for the PS_{132} series.

3.3.2. Boundaries of Other Morphological Transitions. For the series of diblocks with PS_{132} (see Figure 1B−D), generally, the morphological boundaries shift to higher water contents as the PAA block length increases. For the copolymer PS_{132}-*b*-PAA_{16} (Figure 1B), however, the behavior is different at higher water contents because vesicles appear right after the rods + open-bilayers region rather than only open bilayers. In comparing the rod + open-bilayer/vesicle boundary in Figure 1B with the rod + open-bilayer/open-bilayer boundaries in Figure 1C,D, it is found that the boundary in Figure 1B appears at higher water contents than those for copolymers with the longer PAA blocks (Figure 1C,D). The other series of copolymers with PS_{49} show more regular changes with increasing PAA block length. Both diagrams share the same number of phases and thus the same number of morphological boundaries. With increasing PAA block length, all the boundaries move to higher water contents. It is clear that the increase in the corona repulsion with increasing PAA block length causes the changes in the morphological boundaries here. In comparison to the effect of the total block length, the effect of the PAA block is less complicated and easier to understand because the PS block length is kept constant in the study.

3.3.3. Various Morphologies Involving Bilayer Structures. It is known that the corona-forming block length influences the aggregate morphologies of diblock copolymers.[2] It is of interest to see specifically how the aggregate morphologies vary with the PAA block length for copolymers with short PS blocks at different water contents. In parallel with the effect of the total block length, a change in the PAA block length alone does not affect the sequence of the observed morphologies at low water contents. Thus, spheres and rods always appear first. At relatively high water contents, however, the morphologies involving bilayer structures do vary with changing PAA block length.

For the series of copolymers with PS_{132}, two aggregate morphologies are shown in Figure 9 for 10.0 wt % PS_{132}-*b*-PAA_{16}, in Figure 4 for 2.00 and 10.0 wt % PS_{132}-*b*-PAA_{20}, and in Figure 7 for 2.00 and 10.0 wt % PS_{132}-*b*-PAA_{26}. At low polymer concentrations (see Figure 4A−D and Figure 7A−C), the aggregate morphologies do not show appreciable differences for different PAA block lengths at comparable water contents. For example, at low water contents open bilayers appear (see Figures 4A and 7A), while at high water contents vesicles are seen (Figures 4D and 7C). By contrast, at relatively high polymer concentrations, i.e., 10.0 wt %, the aggregate morphologies can change appreciably with increasing PAA block length. For the copolymer PS_{132}-*b*-PAA_{16} (Figure 9A), a mixture of bilayers and rods is present at 16.5 wt % of water. As the water content increases to 40.0 wt % (Figure 9B), the aggregates change directly to pure vesicles, without going through the open bilayer

stage (compare Figure 9 with Figures 4 and 7). As the PAA block increases to 20 repeat units (PS_{132}-*b*-PAA_{20}), at 40 wt % water (Figure 4H), a mixture of various morphologies, including open bilayers, vesicles, and HHHs, is present. For the longest PAA block (PS_{132}-*b*-PAA_{26}) at 40 wt % water, only vesicles appear (Figure 7F). Since the corona repulsion increases with increasing PAA block length, the aggregate morphologies should change in the direction of inverted structures to bilayers and to spheres at the same polymer and water content. The morphological changes from copolymers PS_{132}-*b*-PAA_{20} to PS_{132}-*b*-PAA_{26} follow the above principle. For the copolymer PS_{132}-*b*-PAA_{16} with the shortest PAA block, more inverted structures are expected to appear but are not seen (Figure 9B).

The PAA effect on the aggregate morphologies was also studied for the other series of copolymers with PS_{49}. As seen from Figures 5 and 8, with increasing PAA block length, the aggregate morphologies change from inverted structures (see Figure 5C) to bilayers (see Figure 8D) at high water contents; this change is clearly due to the increase in the corona repulsion. At a relatively low water content (ca. 23 wt %), the lamellar morphology does not change appreciably for the copolymers with different PAA blocks (see Figures 5A and 8A).

As shown in the study of the total block length effect on aggregate morphologies, at low polymer concentrations, vesicles are generally the main morphology and, in many cases, the only morphology. One can then compare the effective hydrodynamic radius of the vesicles prepared from copolymers with various PAA block lengths. As seen in Figure 6, for both series of copolymers, the longer the PAA block length, the larger the effective hydrodynamic radii of the vesicles. The effective hydrodynamic radii at 1 wt % polymer and the *z* average hydrodynamic radii (R_{h0}) of the vesicles are listed in Table 1.

3.4. Effect of the PS Block Length. The effect of the PS block length for copolymers with the same PAA block length was not examined in this study, since it is very difficult to synthesize copolymers with the same PAA block length but different PS block lengths. Also, the range of PS block lengths is small if one wishes to obtain aggregates of a specific morphology for a particular PAA block length. For example, for a PAA block of 50 repeat units, the whole range of morphologies is seen only for copolymers with in the range of PS block lengths from ca. 250 to ca. 350 units. Also, preliminary experiments have shown that the aggregate morphologies are basically the same as those described previously and can thus be extrapolated from the results of the previous work.[10] For example, for copolymers for which the PS block length is increased from 250 to 350 units, spheres, rods, and vesicles are all present in the phase diagrams, but the corresponding morphological boundaries move to lower water contents. Also, the ratio of the block lengths is far more important than the absolute block length in the formation of specific morphologies. The investigation of the effect of the total block length for copolymers with a similar PAA content provides more information, which also reflects the PS effect on the morphological phase diagram. On the basis of the results of that investigation, one can predict the PS effect for copolymers with shorter PAA block lengths. For example, as the PS block increases from ca. 30 to ca. 100 units for copolymers with 10 units of PAA, the morphologies will change from spheres, rods, and bilayers to spheres, rods, bilayers, and vesicles. Also, the corresponding morphological boundaries will shift to lower water contents.

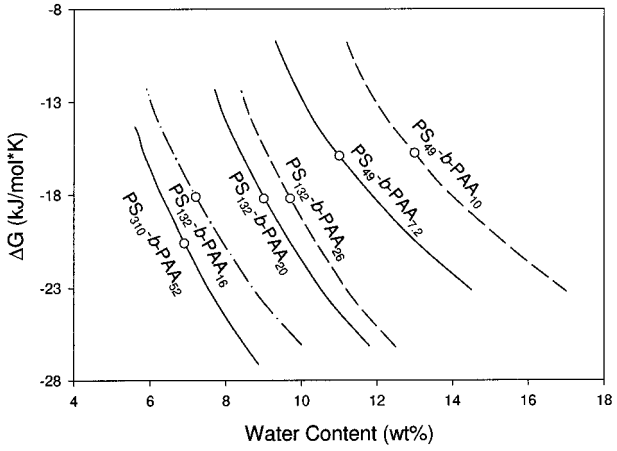

Figure 10. Gibbs free energies of the single-chain to sphere transition as a function of the water content. Circles represent values of free energies of the single-chain to sphere transition for 1.0 wt % copolymer.

3.5. Estimation of Gibbs Free Energies of the Single Chain to Sphere Transition. From the single-chain/sphere boundaries in the morphological phase diagrams, the Gibbs free energies were estimated on the basis of the closed association model. The detailed estimation process has been described in the previous phase diagram study.[10] Figure 10 shows the free energy of the single chain to sphere transition as a function of the water content at 25 °C. Since all of the curves originate from the single-chain/sphere boundary, they start and end at the same polymer concentrations.

The three solid lines in Figure 10 represent the effect of the total block length on the free energy for copolymers with ca. 13% PAA. As the total block length decreases, the free energy at the same water content becomes less negative, and thus the single chain to sphere transition should be more difficult. For the same polymer concentration, the free energy also becomes less negative with decreasing total block length. This can be seen clearly from the circular symbols, which represent the free energy changes for 1.0 wt % polymer solutions. The results from the other series of copolymers with 17% PAA show the same trends, as seen from the dashed lines in Figure 10.

The PAA effect on the free energy is also shown in Figure 10. Lines 2−4 from the left show the results for the PS_{132} series of copolymers, while the two lines at the far right show the results for the PS_{49} series of copolymers. For both series, the free energy becomes less negative with increasing PAA block length at the same water content. The overall changes in the free energy are not as significant as those for the total block length effect. Also, at the same polymer concentration, the free energy does not show an appreciable change with increasing PAA block length (see circles on the lines).

4. Conclusion

The block length dependence of morphological phase diagrams is described in detail for the ternary system of PS-*b*-PAA/dioxane/water. Six copolymers with various PS and PAA block lengths were studied. These morphological phase diagrams cover the range of water contents from 0 to 50 wt % and the range of copolymer

concentrations from 0.1 to 10 wt %. For all the systems investigated here, the sequence of copolymer structures in solution follows the order of single chains, spheres, sphere and rod mixtures, rods, rod and bilayer mixtures, pure bilayers, and for copolymers with short PS blocks, mixtures of bilayers and inverted structures. The bilayers here include vesicles, lamellae, and other structures.

The effect of the total block length on the morphological boundaries and aggregate morphologies was examined using two series of copolymers. With decreasing total block length, the boundaries of various morphological transitions, in general, shift to higher water contents due to the increase of the interfacial tension between the PS block and the solvent. The actual form of the bilayer structures, i.e., planar lamellae, vesicles, and other structures, also depends on the total block length. It is found that it is easier to form vesicles from copolymers having relatively long PS blocks than those having short PS blocks. This study provides the first experimental evidence that vesicles can form spontaneously in long chain block copolymer systems with high bending moduli, while planar lamellae are favored for short chain block copolymers with low bending moduli. Thus, our results reinforce the conclusion of the SPA model. Furthermore, it was found that spontaneous vesicle formation is not simply related to the total molecular weights of the copolymer but is more directly related to the core-forming block length. It was also found that the planar lamellae formed from copolymers with short total block lengths can change to vesicles at high water contents. In addition, inverted structures are found from copolymers with short PS blocks at relatively high polymer concentrations and high water contents.

The effect of the PAA block length on the morphological phase diagrams was also examined using two series of copolymers. With increasing PAA block length, all morphological boundaries shift to higher water contents due to the increase of the interaction of the corona with the solvent. The effect of the PS block length is also discussed. It is found that both PS and PAA effects alone on the morphologies are not as significant as the total block length effect. In addition, on the basis of the closed association model, the Gibbs free energies were estimated for the single-chain/sphere transition from the morphological boundaries. As expected, it is found that at the same water content the free energy increases both with decreasing total block length and with increasing PAA block length.

Acknowledgment. We thank the Petroleum Research Fund, administered by the American Chemical Society, for the support of this work.

References and Notes

(1) Tuzar, Z.; Kratochvil, P. *Adv. Colloid Interface Sci.* **1976**, *6*, 201. In *Surface and Colloid Science*; Matijievic, E., Ed.; Plenum Press: New York, 1993; Vol. 15, p 1. Price, C. In *Developments in Block Copolymers*; Goodman, I., Ed.; Applied Science Publishers: London, 1982; Vol. 1, p 39. Selb, J.; Gallot, Y. In *Developments in Block Copolymers*; Goodman, I., Ed.; Applied Science Publishers: London, 1985; Vol. 2, p 27. Riess, G.; Hurtrez, G.; Bahadur, P. *Encyclopedia of Polymer Science and Engineering*, 2nd ed.; Wiley: New York, 1985; Vol. 2, p 324. Halperin, A.; Tirrell, M.; Lodge, T. P. *Adv. Polym. Sci.* **1992**, *100*, 31.

(2) Zhang, L.; Eisenberg, A. *Science* **1995**, *268*, 1728; *J. Am. Chem. Soc.* **1996**, *118*, 3168.

(3) Zhang, L.; Yu, K.; Eisenberg, A. *Science* **1996**, *272*, 1777. Zhang, L.; Eisenberg, A. *Macromolecules* **1996**, *29*, 8805.

(4) Spatz, J. P.; Mössmer, S.; Möller, M. *Angew. Chem., Int. Ed. Engl.* **1996**, *35*, 1510. Spatz, J. P.; Sheiko, S.; Möller, M. *Macromolecules* **1996**, *29*, 3220. Guo, A.; Liu, G.; Tao, J. *Macromolecules* **1996**, *29*, 2487. Ding, J.; Liu, G. *Macromolecules* **1997**, *30*, 655. Massey, J.; Power, K. N.; Manners, I.; Winnik, M. A. *J. Am. Chem. Soc.* **1998**, *120*, 9533. Kabanov, A. V.; Bronich, T. K.; Kabanov, V. A.; Yu, K.; Eisenberg, A. *J. Am. Chem. Soc.* **1998**, *120*, 9941.

(5) Zhang, L.; Shen, H.; Eisenberg, A. *Macromolecules* **1997**, *30*, 1001.

(6) Zhang, L.; Bartels, C.; Yu, Y.; Shen, H.; Eisenberg, A. *Phys. Rev. Lett.* **1997**, *79*, 5034.

(7) Yu, Y.; Eisenberg, A. *J. Am. Chem. Soc.* **1997**, *119*, 8383. Yu, Y.; Zhang, L.; Eisenberg, A. *Macromolecules* **1998**, *31*, 1144.

(8) Zhang, L.; Eisenberg, A. *Polym. Adv. Technol.* **1998**, *9*, 677.

(9) Cameron, N. S.; Corbierre, M. K.; Eisenberg, A. *Can. J. Chem.* **1999**, *77*, 1311.

(10) Shen, H.; Eisenberg, A. *J. Phys. Chem. B* **1999**, *103*, 9473.

(11) Chen, L.; Shen, H.; Eisenberg, A. *J. Phys. Chem. B* **1999**, *103*, 9488.

(12) Hajduk, D. A.; Harper, P. E.; Gruner, S. M.; Honeker, C. C.; Kim, G.; Thomas, E. L.; Fetters, L. J. *Macromolecules* **1994**, *27*, 4063. Matsen, M. W.; Bates, F. S. *Macromolecules* **1996**, *29*, 7641.

(13) Yoshikiyo, M. *Micelles: Theoretical and Applied Aspects*; Plenum Press: New York, 1992. Davis, H. T. *Colloids Surf., A* **1994**, *91*, 9.

(14) Kaler, E. W.; Murthy, A. K.; Rodriguez, B. E.; Zasadzinski, T. A. *Science* **1989**, *245*, 1371.

(15) Wanka, G.; Hoffmann, H.; Ulbricht, W. *Macromolecules* **1994**, *27*, 4145.

(16) Alexandridis, P.; Holmqvist, P.; Lindman, B. *Colloids Surf., A* **1997**, *130*, 3. Alexandridis, P.; Olsson, U.; Lindman, B. *Langmuir* **1998**, *14*, 2627.

(17) Safran, S. A.; Pincus, P.; Andelman, D. *Science* **1990**, *248*, 354.

(18) Shen, H.; Zhang, L.; Eisenberg, A. *J. Phys. Chem. B* **1997**, *101*, 4697.

(19) Hautekeer, J. P.; Varshney, S. K.; Fayt, R.; Jacobs, C.; Jerome, R.; Teyssie, Ph. *Macromolecules* **1990**, *23*, 3893.

(20) Tian, M.; Qin, A.; Ramireddy, C.; Webber, S. E.; Munk, P.; Tuzar, Z.; Procházka, K. *Langmuir* **1993**, *9*, 1741.

MA991161U